

# Passive imaging of cavitation acoustic emissions with ultrasound arrays

Vasant A. Salgaonkar,<sup>a</sup> Saurabh Datta,<sup>b</sup> Christy K. Holland,<sup>a</sup>  
and T. Douglas Mast<sup>a</sup>

<sup>a</sup>*Department of Biomedical Engineering, University of Cincinnati, Cincinnati, OH*

<sup>b</sup>*Siemens Medical Solutions USA Inc., Mountain View, CA*

**Abstract.** A method is presented for imaging emissions from active microbubbles using an ultrasound array. Since bubble activity plays a role in ultrasound ablation, monitoring cavitation may assist in therapy guidance. This is often achieved by listening passively for bubble emissions with a single-element transducer. Such schemes do not capture the variation in cavitation in form of a two dimensional (2D) map or image. The technique presented here obtains spatial information by creating images solely from the beamformed cavitation-emission energy received by an array, dynamically focused at multiple depths. An analytic expression was derived for these passive images by numerically solving the Rayleigh-Sommerfield integral under the Fresnel approximation. To test accuracy in mapping of localized emissions, a 192-element array was employed to passively image scattering of 520-kHz ultrasound by a 1-mm steel wire. The wire position was estimated from the passive images with rms error 0.9 mm in azimuth and 17.2 mm in range. Bubbles created in air-saturated saline sonicated at 520-kHz were imaged passively from both ultraharmonic and broadband emissions. Good agreement was found between azimuthal brightness distributions of the passive images and B-scan images of the bubble cloud. Broadband emission images from *ex vivo* bovine liver sonicated with 2.2-MHz focused ultrasound were also recorded. The image brightness along the array azimuth was consistent with the source beam profile. This indicates the possibility of mapping therapeutic ultrasound beams *in situ*.

**Keywords:** acoustic cavitation, array beamforming, acoustical medical instrumentation

**PACS:** 43.35.Ei, 43.60.Fg, 43.80.Vi

## INTRODUCTION

A method to spatially resolve acoustic emissions from active bubbles using ultrasound arrays is presented. Acoustic cavitation is known to play an important role in ultrasound-based therapies including shock-wave lithotripsy [1], thrombolysis [2], targeted drug delivery [3], and thermal ablation [4]. During ultrasound ablation, cavitation results in enhanced tissue heating [5], but also complicates energy deposition and distorts ablative lesion shapes [6]. Monitoring of ablation by measuring bubble activity, typically with single-element transducers [7], could be improved if spatial variation in cavitation was captured. Ultrasound arrays have been employed with some success in imaging bubbles during high-intensity focused ultrasound (HIFU) exposures in B-mode imaging [8] and as passive cavitation detectors [9]. In this paper, a method for passive cavitation imaging using ultrasound arrays is introduced, analyzed, and illustrated by example simulations and experiments.

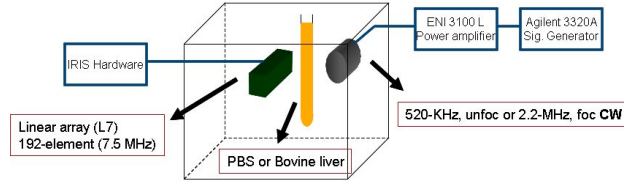


**FIGURE 1.** Experimental setup: CW ultrasound sources sonicate a 1 mm steel wire, PBS solution, and bovine liver, while a 192-element linear array captures passive images.

## THEORY

In the passive cavitation imaging method presented here, acoustic emissions from cavitating bubbles are detected by a linear ultrasound array. These passively received signals are then beamformed in real time by delay-and-sum methods common to clinical B-scan imaging systems. To model this imaging method, a bubble is represented as a point source at position  $\mathbf{r}_s$ . The frequency-domain signal received by an array subaperture is modeled as an integral of the point-source field over the receiver surface  $S_0$ ,

$$S(\omega) = \oint \frac{e^{ik|\mathbf{r}_0 - \mathbf{r}_s|}}{|\mathbf{r}_0 - \mathbf{r}_s|} dS_0. \quad (1)$$

The brightness of a passive cavitation image at the coordinate  $(Y, Z)$  is then given by the beamformed acoustic emission energy received by a subaperture focused at that point. For an array subaperture modeled as a continuous receiver with a fixed focus in the elevation ( $x$ ) direction and a width  $2b$  in the array ( $y$ ) direction, the beamformed emission for a single source is given under the Fresnel approximation [10] as

$$S(\omega, Y, Z) = \frac{f(x_s, z_s)}{\sqrt{1 - \frac{z_s}{Z}}} \left( \mathbf{F} \left[ \frac{k[(y_s - Y) - (\frac{z_s}{Z} - 1)b]}{\sqrt{\pi k(\frac{z_s}{Z} - 1)z_s}} \right] - \mathbf{F} \left[ \frac{k[(y_s - Y) + (\frac{z_s}{Z} - 1)b]}{\sqrt{\pi k(\frac{z_s}{Z} - 1)z_s}} \right] \right), \quad (2)$$

where  $(x_s, y_s, z_s)$  is the bubble position,  $k$  is the wavenumber  $\omega/c$ ,  $\mathbf{F}$  is the complex Fresnel integral, and terms not dependent on the image coordinate  $(Y, Z)$  have been incorporated into the function  $f(x_s, z_s)$ . The final point-spread function (passive cavitation image for a single point source) is then given by the total beamformed emission energy for all frequencies of interest,

$$I(Y, Z) = \sum_i |q(\omega_i) S(\omega_i, Y, Z)|^2, \quad (3)$$

where  $q(\omega_i)$  is the source strength at each frequency  $\omega_i$ . Alternatively, passive cavitation images can be simulated by computing the emission signal received by each element using the Fresnel approximation, and synthetically focusing the received signals by standard delay and sum methods.

## EXPERIMENTS

Passive cavitation imaging was tested here in a series of *in vitro* experiments. A glass tank was filled with deionized, degassed ( $\%O_2 < 35$ ), filtered (particle size  $< 0.2 \mu\text{m}$ )

water. Passive images were obtained using a 192-element linear array with a 7.5 MHz center frequency and a total aperture size of  $42 \times 7 \text{ mm}^2$  (L7 array and Iris imaging system, Guided Therapy Systems). For an image frame, 192 beamformed RF emission signals, each obtained by real-time focusing at 16 equally-spaced depths, were sampled at 33.3 MHz by a 14-bit, PC-based A/D card (Compuscope CS 14200, Gage Applied). For each exposure, 38 sequential frames were acquired at 28 fps and stored. To form passive cavitation images, power spectra were computed for each receive focal zone and filtered to create separate images for distinct frequency bands, including ultraharmonic emissions due to stable cavitation and broadband emissions due to inertial cavitation [11]. The filtered energy was summed in each focal zone over all 38 frames to obtain a single passive image with  $192 \times 16$  points.

Passive imaging performance was first evaluated using ultrasound scattered from a 1 mm steel wire. Continuous-wave sonication was performed by a 520 kHz, 1" diameter source (Panametrics C302) with peak-negative pressure amplitude 0.123 MPa (0.241 MPa peak-to-peak). The wire was placed orthogonal to the image plane to approximate a point source. Scattering of the source (520 kHz) harmonics between 5.2–9.36 MHz (covering the bandwidth of the L7 array) was passively imaged using subapertures designed to maintain a constant f-number (subaperture width divided by focal depth) of 7.1. The passive image is consistent with the corresponding simulated image of a point source, for both the “idealized” subaperture and time-delay focusing formulations (Figure 2). To assess spatial resolution of the passive images, the wire was moved to 21 distinct positions distributed throughout the image plane. To estimate the target position, energy of each beamformed signal was integrated over all depths, and the target azimuth was estimated as the position of peak integrated energy (rms error 0.9 mm). The target range was estimated as the position of peak signal amplitude at this azimuth (rms error 17.2 mm).

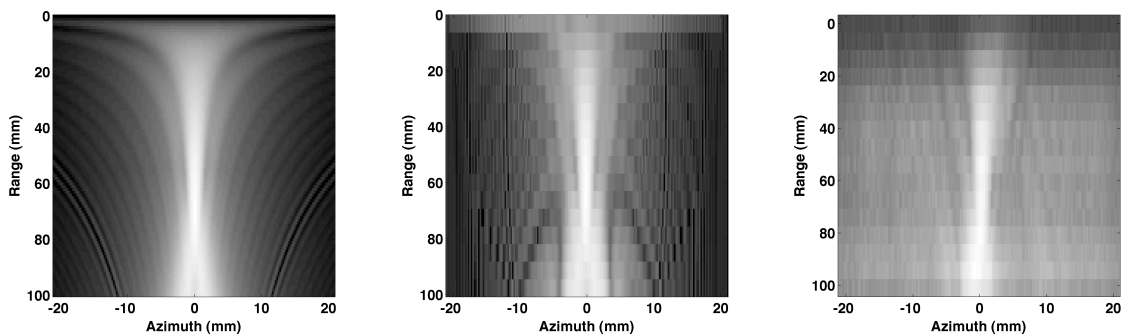


**FIGURE 2.** Simulated and experimental passive images of a point source at position (0 mm, 55 mm), obtained using a constant f-number and shown with 40 dB dynamic range. Left: simulated image for idealized aperture. Center: simulated image for linear array with time-delay focusing. Right: measured image of scattering from 1-mm wire.

In order to test the spatial correlation of passive cavitation images with confirmed bubble activity, cavitation was created by sonicating phosphate-buffered saline (PBS) solution in a 30-mm latex condom with 520-kHz, CW ultrasound (Panametrics C302). No bubbles were evident by B-scan imaging until the peak-negative sonication pressure exceeded 0.125 MPa (0.245 MPa peak-to-peak pressure), after which echogenic bubbles

would accumulate on the distal wall of the condom. Passive images were formed, using a constant 64-element subaperture size, from ultraharmonic and broadband frequency components (Figure 3). The azimuthal position of the bubble cluster is seen to correspond with the region of greatest bubble activity. For quantitative comparisons, a region of interest (ROI) containing the bubble cluster on the B-scan was selected, spanning 15 mm in depth and the entire image in the array direction. The depth-integrated signal energy within this ROI was computed for both the B-scan and broadband-emission images. The spatial correlation between these two 192-point energy distributions was  $> 0.85$  for each of 10 trials. It should be noted that the B-scan did not show a visible change in the size and position of the bubble cloud during the image acquisition.

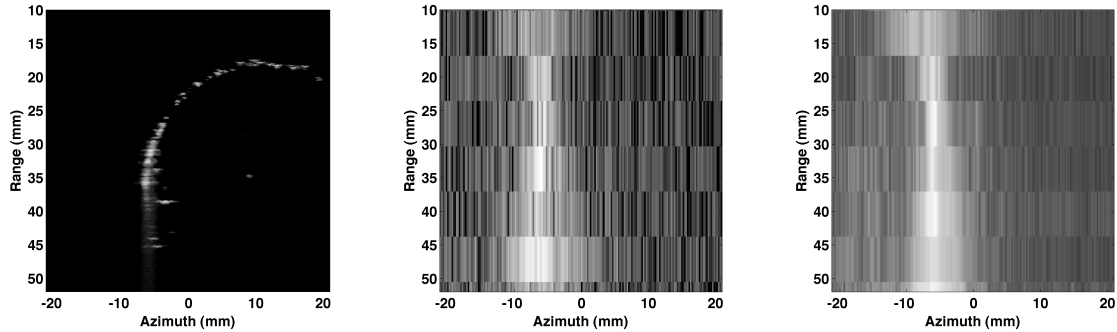


**FIGURE 3.** Passive cavitation imaging in saline solution for sonication at 520-kHz with 0.137 MPa peak negative pressure (0.31 MPa peak-to-peak). Left: B-scan showing a cavitating bubble cloud. Center: co-registered passive cavitation image formed from ultraharmonic emissions (6.5 MHz, or 12.5 times the fundamental frequency). Right: co-registered passive cavitation image formed from broadband emissions (6.3-6.7 MHz).

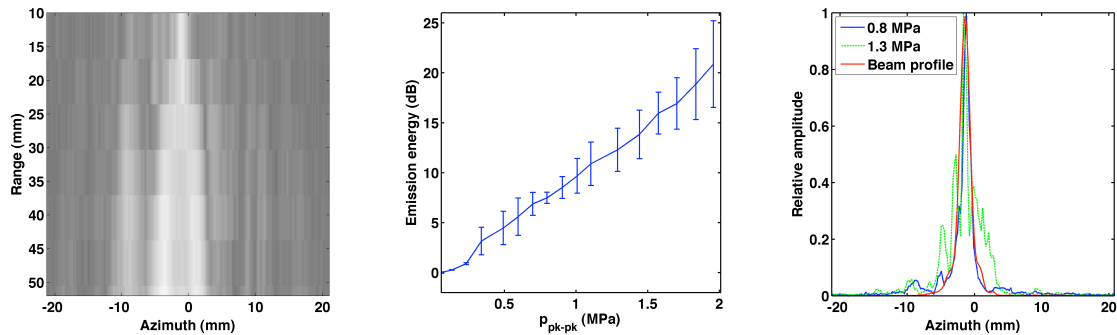


**FIGURE 4.** Passive cavitation imaging using broadband emissions from bovine liver tissue sonicated at 2.2 MHz. Left: passive image at 0.8 MPa peak-to-peak pressure (0.38 MPa peak negative pressure). Center: spatially-integrated emission energy as a function of sonication amplitude (mean  $\pm$  standard deviation,  $N = 4$ ). Right: representative comparison of emission amplitude at 20 mm depth with measured beam profile.

Finally, *ex vivo* bovine liver was exposed to a 2.2-MHz,  $4 \times 15$  mm<sup>2</sup> focused source (UTX IX327), aligned with the propagation direction orthogonal to the image plane. The source focus was aligned to the image plane on the array axis at a depth of 20 mm using a pulse-echo technique. The sonication amplitude was increased from 0–1.96 MPa peak-to-peak pressure, corresponding to 0–0.58 MPa peak-negative pressure, and passive

images were captured with a constant 64-element subaperture for 4 tissue samples of size  $7 \times 3 \times 3 \text{ cm}^3$  (Figure 4). While emissions detected by the linear array did not show a significant signal at ultraharmonics of the source frequency, the broadband energy (8–10 MHz) increased monotonically with the sonication amplitude. The azimuthal position of the source focus could be visually identified from the broadband emission images. The passive image brightness pattern at the source focus depth was consistent with the beam profile along the array azimuth, as measured by a scanning hydrophone system. The passive image brightness pattern is seen to broaden with sonication amplitude, possibly because of cavitation activity within sidelobes in the transducer beam pattern.

## CONCLUSIONS

A method for passive cavitation imaging using linear ultrasound arrays has been introduced and its analytic point-spread-function has been derived. Experiments substantiate that passively detected acoustic emissions can be spatially resolved into separate images for different frequency ranges. Acoustic emission sources can be localized more accurately in the array direction than in the range direction. In experiments with tissue, the broadband energy distribution along the azimuth corresponded with the beam shape of the focused source. Passive cavitation imaging could potentially enable direct visualization of therapeutic ultrasound beams *in situ*.

**Acknowledgments:** This research was supported by a University of Cincinnati College of Medicine Dean's Bridge Funding Program Award and NIH grant R01-NS047603. Jonathan Kopecheck, Mark Burgess, and Eileen Slavin are thanked for help during the experiments.

## REFERENCES

1. Cleveland RO. Acoustics of shock wave lithotripsy. Renal Stone Disease, 1<sup>st</sup> Annual International Urology Research Symposium 2007; 311–316.
2. Datta S, Coussios CC, McAdory LE, Tan J, Porter T, De Courten-Myers G, Holland CK. Correlation of cavitation with ultrasound enhancement of thrombolysis. *Ultras Med Biol* 2006; 32:1257–1267.
3. Hynynen K. Ultrasound for drug and gene delivery to the brain. *Adv Drug Del Rev* 2008; 60:1209–1217.
4. ter Haar GR, Daniels S. Evidence for ultrasonically induced cavitation *in vivo*. *Phys Med Biol* 1981; 26:1145–1149.
5. Coussios CC, Farny CH, ter Haar GR, Roy RA. Role of acoustic cavitation in the delivery and monitoring of cancer treatment by high-intensity focused ultrasound (HIFU), *Int J Hyperthermia* 2007; 23:105–120.
6. Watkin NA, ter Haar GR, Rivens I. The intensity dependence of the site of maximal energy deposition in focused ultrasound surgery. *Ultras Med Biol* 1996; 22:1690–1698.
7. Mast TD, Salgaonkar VA, Karunakaran C, Besse JA, Datta S, Holland CK. Acoustic emissions during 3.1 MHz ultrasound bulk ablation *in vitro*. *Ultras Med Biol* 2008; 34:1434–1448.
8. Rabkin BA, Zedric V, Vaezy S. Hyperecho in ultrasound images of HIFU therapy: Involvement of cavitation. *Ultras Med Biol* 2005; 31:947–956.
9. Farny CH. *Identifying and monitoring the roles of cavitation in heating from high-intensity focused ultrasound* (PhD dissertation, Boston University, 2007).
10. Mast TD. Fresnel approximations for ultrasonic fields of rectangularly symmetric sources. *J Acoust Soc Am* 2007; 121:311–3322.
11. T. G. Leighton, *The Acoustic Bubble* (Academic Press, 1994), ch. 4.